Eur. Phys. J. B **8**, 179–193 (1999)

THE EUROPEAN PHYSICAL JOURNAL B

EDP Sciences

Spatial versus quantum confinement in porous amorphous silicon nanostructures

R.B. Wehrspohn[a], J.-N. Chazalviel, F. Ozanam, and I. Solomon

Laboratoire de Physique de la Matière Condensée, CNRS-École Polytechnique, 91128 Palaiseau Cedex, France

Received: 3 August 1998

Abstract. Light-emitting porous amorphous silicon has been produced by anodization in HF of hydrogenated amorphous silicon films. The maximal thickness of the porous films is limited by the onset of an instability which results in the formation of large channels short-circuiting the amorphous layer. This is due to the high resistivity of the amorphous silicon films as compared to that of the electrolyte. Confinement effects on the electron wavefunction are analyzed *in situ* using photoluminescence measurements in hydrofluoric acid and compared to those observed in porous crystalline silicon. For crystalline silicon, a huge blue shift of the photoluminescence is observable upon reducing the size of the structures by photo-etch, showing clear evidence of quantum confinement effects in this material. No shift has been observed when carrying out the same experiment with amorphous silicon. This indicates that the extent of the wavefunction in the bandtail states involved in luminescence is too small to be sensitive to confinement down to the minimum sizes of our porous material ($\sim$ 3 nm). Measurements of the width and the temperature dependence of the photoluminescence demonstrate that the Urbach energy does not change upon increasing the porosity, *i.e.*, upon decreasing the size of the *a*-Si:H nanostructures, in contradiction with what has been reported in ultrathin *a*-Si:H multilayers.

PACS. 78.55.Mb Porous materials – 78.66.Jg Amorphous semiconductors; glasses; nanocrystalline materials – 81.05.Rm Porous materials; granular materials

1 Introduction

Bustarret *et al.* [1–3] first reported light emission from anodized amorphous silicon layers. However, their *a*-Si:H films were obtained under unconventional deposition conditions and the luminescence was spatially inhomogeneous. Several other groups tried to make *a*-Si:H microporous but did not succeed [4,5]. Recently, our group obtained strongly luminescent porous silicon by anodization of device-grade amorphous silicon films [6]. Independently, Estes *et al.* [7] have also obtained luminescent porous *a*-Si:H in line with our results. The maximal thickness of the porous *a*-Si:H films obtained is rather small, 0.4 μm [6], and even smaller (0.08 μm) for those of Estes *et al.* [7]. We have attributed this limitation to an instability arising from the high resistivity of amorphous silicon [8]. Because the amount of material is limited, the total photoluminescence (PL) is rather weak but the intensity for the same thickness (related to the quantum efficiency) is not much smaller than that of porous crystalline silicon.

For porous crystalline silicon films, photoluminescence properties have been studied extensively since the first observation of the very intense PL band at around 2 eV in 1990 (see *e.g.*, review [9]). The blue shift of the PL peak energy (from E_g = 1.1 eV to $\sim$ 2 eV) has been interpreted in terms of quantum confinement effects (QCE) by several groups, since the size of the silicon structures is in the range of 20 to 30 Å, *i.e.*, a size for which significant confinement effects on the electron wavefunction are expected. The QCE interpretation has been experimentally verified by *in situ* photoluminescence experiments in hydrofluoric acid [10], resonantly excited photoluminescence measurements [11] and spectral shifts of electroluminescence in an electrolyte [12].

Radiative recombination properties in *a*-Si:H nanostructures and confinement effects have been investigated theoretically as well as experimentally by many groups [13–21]. Nevertheless, it is still a matter of debate to what extent the localized and the extended states are affected by quantum confinement effects. The localization length in amorphous silicon has been estimated by Mott [13] to be about 2 to 3 atomic distances, *i.e.*, about 6–7 Å. Since PL arises from thermalized electron-hole pairs in the *localized* states, no confinement effects on the PL peak energy are expected for sizes of the nanostructures larger than this critical size. Experimentally, in *a*-Si:H/*a*-Si:N:H [14] and *a*-Si/*a*-SiO_2 [15] multilayers, a blue shift of the PL peak energy has been observed upon reducing the *a*-Si:H layer thickness. This shift has been interpreted in terms

[a] *Present address:* Philips Research Laboratories, Redhill, Surrey, RH1 5HA, UK.
e-mail: wehrspoh@prl.research.philips.com

of quantum confinement effects on the electron wavefunction in *a*-Si:H. Another size effect has been reported as inducing a broadening of the Urbach energy [17,18]. This increase of the Urbach energy has been explained by a significant shift of the mobility edge to higher energies, the lowest localized states being not or less affected [14,19].

Most of the previous investigations on size effects in amorphous silicon are based on the study of amorphous silicon ultrathin multilayers. It is known that these materials do not have perfect interfaces (the barrier material is mostly amorphous silicon oxide or silicon nitride) [20]. Moreover, ultrathin deposits of *a*-Si:H do not have the same material properties as bulk *a*-Si:H [21]. With respect to these problems, specific to multilayers, porous *a*-Si:H [6] has several advantages: this material has the same atomic structure as bulk amorphous silicon since it is obtained from it by anodic etching, and it has no interface states because the surface of the silicon wires is perfectly passivated by hydrogen [22]. In the present article, we show that *in situ* photoluminescence measurements allow a direct comparison between confinement effects in crystalline and amorphous silicon. The analysis of the shape of the spectrum and its temperature dependence as a function of size brings further information on the radiative recombination properties to be compared to that of multilayer measurements.

This paper reviews our recent work on porous *a*-Si:H and porous *c*-Si [6,8,10,22–25], confirms some preliminary measurements and gives complementary results. It will be organized as follows: after a description of the preparation and experimental techniques, we briefly review the properties of the instability during anodization, the simulation of this phenomenon by a linear stability analysis and finally give some possible solutions to avoid the onset of this instability. A complete analysis of the PL properties of porous *a*-Si:H (*a*PS) is presented with respect to confinement effects on the localized *and* the extended states. In order to analyze the confinement effects on the localized states, *in situ* PL experiments are presented and the difference in the recombination mechanisms between crystalline and amorphous porous silicon is discussed. The evolution of the PL peak energy as a function of the size of the structures is discussed. In the next section, size effects on the Urbach energy are investigated, analyzing the width of the PL spectrum and the temperature dependence of the PL efficiency. Finally, PL of porous *a*-Si:H is compared to that of ultrathin *a*-Si:H multilayers.

2 Preparation and experimental techniques

2.1 Starting material for anodization: hydrogenated amorphous silicon

Hydrogenated amorphous silicon films are produced by rf-plasma decomposition of pure silane SiH_4 in a capacitively-coupled reactor at 13.56 MHz. Normal deposition conditions are: total pressure, 50 mtorr; gas flow rate, 2 l/h; rf power density, 0.15 W/cm^2; substrate temperature, 250 °C. These parameter values are known to produce a homogeneous, low density-of-state amorphous material, far from the conditions of microcrystalline silicon formation [26]. Boron doping is obtained by injecting a small amount of an admixture of diborane gas and hydrogen (3% of B_2H_6 in H_2) in the plasma. The films were deposited on optically polished stainless steel substrates ((25× 75× 1) mm^3). The deposition rate was about 4 Å/s for undoped films and up to 6 Å/s for the highly doped samples. In order to provide a good ohmic contact, a very thin heavily boron doped *a*-Si:H film (1000 Å, 2% B_2H_6) was first deposited on the stainless steel substrate.

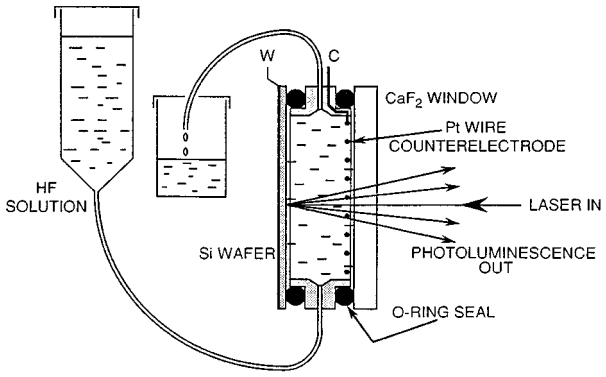

Fig. 1. Schematic picture of the electrochmical cell used for anodization of silicon and *in situ* photoluminescence analyses.

The undoped amorphous deposited material is of device grade, with a gap defined by $E_{04} = 1.9$ eV, a refractive index $n(\lambda = 0) = 3.4$, an average gap E_{av} of 3.48 eV [27] and a characteristic bandtail energy (Urbach energy ($E_U^{optical}$)) of about 50 meV determined by optical spectroscopy. The defect density of states at the Fermi-level (determined by space-charge limited current measurements) is of about 5×10^{15} cm^{-3} eV^{-1} [28].

Increasing the doping level to about 3% diborane in gas phase, increases the defect density at Fermi-level by several orders of magnitude (up to about 10^{19} cm^{-3} eV^{-1}) [26]. Also, the Urbach energy, which can be taken as a measure of disorder, increases by about a factor of 4 from undoped *a*-Si:H (50 meV) to highly boron doped *a*-Si:H (180 meV) [25].

2.2 Photoluminescence

Photoluminescence of porous amorphous silicon (*a*PS) has been recorded for layers formed under various conditions (*a*-Si:H doping (from 0.1% to 3% boron in gas phase), HF concentration (from 5% to 50%)). The sample was mounted on a copper plate in a vacuum chamber (max. pressure 10^{-3} torr, liquid-nitrogen trapped). The chamber provided optical access to the sample through a SiO_2 window and was fixed on a X-Y translation stage.

In situ PL was performed in the cell where porous silicon had been formed. The cell is schematized in Figure 1. The cell was machined in polytrifluorochloroethylene. The 2-inch *p*-Si wafer, or the *a*-Si:H layer deposited on a stainless steel substrate of the same dimensions, was pressed

against the cell wall with a fluoroelastomer O-ring seal. The opposite side of the cell bore a calcium fluoride window, providing optical access over 40 mm diameter. The counter electrode consisted of parallel, 0.2 mm diameter platinum wires, running along the window. The 4 mm spacing between two wires provided free access for the laser beam used for illumination. The cell was mounted on a X-Y-Z translation stage, allowing fine control of the spot position. Two 0.5 mm inner diameter Teflon tubes were fitted at the top and the bottom of the cell, for filling and emptying the cell, or changing the electrolyte.

The excitation source was a krypton-ion laser (351 nm or 476 nm line). The PL signal was analyzed with a monochromator (27.5 cm focal length, 150 grooves/mm) and recorded with a cryostatically cooled CCD detector (OMA). The spectral sensitivity of the system was calibrated by using a Tungsten lamp at 2850 K.

Time-resolved PL measurements have been carried out at room-temperature and liquid-nitrogen temperature with a pulsed N_2-laser (λ = 337 nm, Δt = 3 ns, μ = 20 Hz). The PL signal was dispersed by a monochromator and detected by a photomultiplier tube, followed by an acquisition system consisting of a Lecroy 9310 AM oscilloscope at 400 MHz. The time resolution is estimated to be about 5 ns.

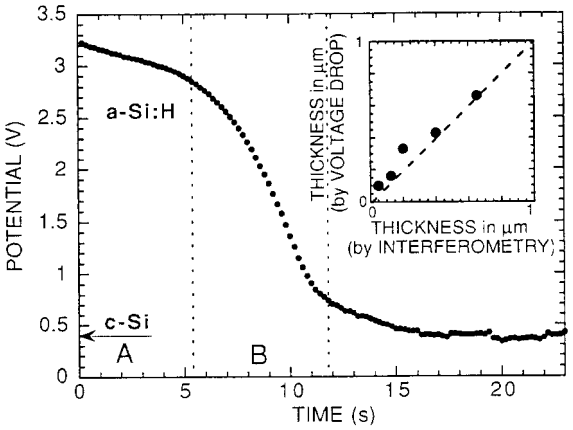

Fig. 2. Potential during the anodization of a-Si:H. The initial potential of about 3 V is due to the ohmic drop in the layer. In region A, the porous layer is formed and the potential decreases linearly with time. In region B, large channels are formed short-circuiting the amorphous layer. Note that for c-Si, the potential is constant during pore formation. The inset shows a comparison of the aPS thickness, as determined from the ohmic drop and by *ex situ* interferometry, for various experimental conditions.

3 Macro-instability during pore formation in a-Si:H

During the anodization of p-type crystalline silicon in HF two different regimes are observable: pore formation and electropolishing. Electropolishing occurs at high current density and low HF concentration, whereas pore formation occurs at low current density and high HF content. By cyclic voltammetry, a quantitative distinction between these two regimes is possible and an overall dissolution reaction of silicon has been determined [29]:

$$2h^+ + \mathrm{Si} + 6\mathrm{HF} \rightarrow \mathrm{SiF}_6^{2-} + 4\mathrm{H}^+ + \mathrm{H}_2 \uparrow$$

i.e., two holes h^+ are needed to dissolve one silicon atom.

Since this is a local reaction, long range order should not be relevant, and the reaction is expected to be the same for amorphous silicon. Indeed, the cyclic voltammetry curves in HF are very similar for both materials [8]. However the preparation of porous silicon from amorphous material is complicated by a new instability, which does not exist with crystalline silicon, and limits severely the thickness of porous material that can be produced to less than 1 μm. This instability affects the electrode potential during dissolution, as shown in Figure 2, where we plot a typical variation of the potential (measured against an Ag/AgCl reference electrode), as a function of anodization time at constant current (J = 10 mA/cm^2, thickness of boron-doped a-Si:H film is about 2 μm).

The initial variation (region A) is the normal regime of formation of amorphous porous material. The larger initial value of the potential and its slight decrease, which are not observed for crystalline silicon, are due to the large resistivity of a-Si:H (even when boron doped) compared to that of the electrolyte. The layer of the formed porous material is filled with electrolyte and the overall resistance of the film decreases. Hence, the potential drop is expected to be proportional to the thickness of porous conductive material formed on the top of the a-Si:H film. This has been quantitatively verified by comparing the thickness determined by the potential drop to the thickness measured by interferometry (inset of Fig. 2).

The new effect is the appearance of a strong and sudden variation of the potential (region B), after which we observe a destruction of the a-Si:H film. Nothing of the sort is observed during anodization of the crystalline material. By comparison with SEM and AFM pictures, the fast decrease of the potential corresponds to a progressive short-circuiting of the a-Si:H layer by growing channels. They tend to be perpendicular to the film, with a diameter of about 100 nm and about one per μm^2.

We explain the different behavior of c-Si and a-Si:H by the resistivities of these two materials. Highly luminescent porous silicon is usually formed on p-type crystalline Si of 1–10 Ωcm resistivity. Boron-doped hydrogenated amorphous silicon exhibits a resistivity ranging from 10^4 to 10^6 Ωcm, depending upon the doping level. This high resistivity makes pores filled with the electrolyte much more conductive (typically $\rho \approx 10{-}100$ Ωcm) than the *bulk* material. This makes the growing of the porous interface unstable after a while: at the end of the conductive tips (*i.e.*, the electro-formed pores), the field enhancement favors carrier collection, thereby causing a preferential dissolution at these locations. This "Laplacian instability" [30] is discussed in more detail in reference [22]: as soon as the resistivity of silicon (ρ_{Si}) is higher

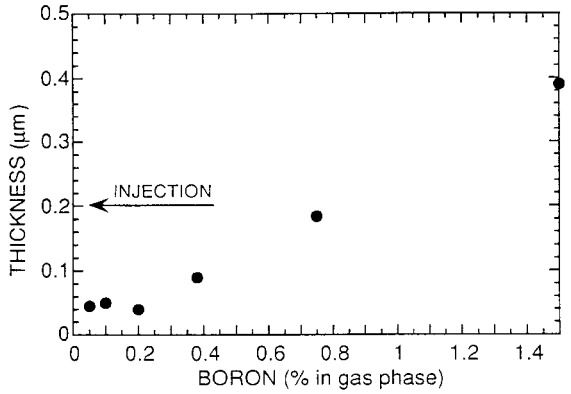

Fig. 3. Maximal thickness of the porous layer as a function of doping. The thickness has been determined by interferometry of the amorphous silicon film before and after anodization. By electrical injection, porous films of increased thickness have been obtained from *undoped* *a*-Si:H (see arrow)

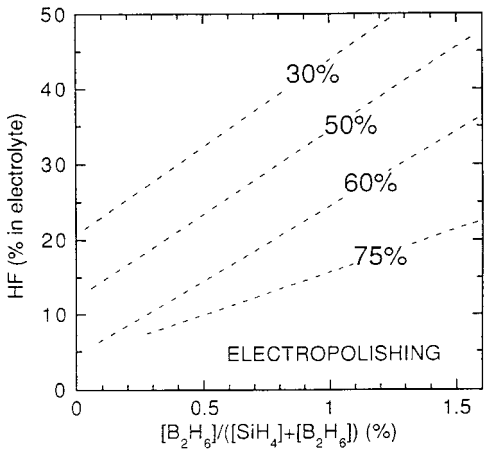

Fig. 4. Iso-porosity curves of porous *a*-Si:H as a function of the doping level and the HF concentration (J =10 mA/cm^2).

than that of the electrolyte (ρ_{el}), the growth front is unstable. The onset of the instability depends on the ratio of the resistivities and it is expected that upon decreasing the resistivity, the onset is shifted to thicker porous layers. The maximal obtainable thickness as a function of the doping level is plotted in Figure 3. Supporting our model, one observes that this maximum thickness increases with doping: porous layers as thick as 0.4 μm can be obtained with highly doped films. It explains also why the first porous amorphous material, as reported by Bustarret *et al.* [1], was obtained from very heavily doped material.

The thin-film geometry of amorphous silicon gives the possibility to produce porous amorphous silicon with undoped device-grade *a*-Si:H, in spite of its high resistivity. This is obtained by electrically injecting holes from the p^+ back contact [23]. In a typical experiment (arrow marked "Injection" in Fig. 3), we have been able to inject a density of holes equivalent to a 1% boron doping, thus producing a layer of undoped porous material of 0.2 μm thickness.

Using the coulometric estimate of the porosity, we have also determined substrate doping and anodization conditions required for obtaining porous amorphous silicon of porosities ranging from 30% to 75% (Fig. 4) [22]. This has been cross-checked for a 35% porosity sample (0.75% B) by X-ray grazing-incidence reflectivity measurement. The trends are quite similar to those of *c*-Si [29] *e.g.*, increasing the HF concentration for a fixed doping level and a fixed current density results in a decrease of the porosity. Further evidence for the similarity between the two types of nanostructure can be found from infrared vibrational spectroscopy. Infrared measurements evidence no surface Si–O bonding on the porous surface. The magnitude of the surface SiH_x signal is of the same order of magnitude as for a *c*PS layer of the same thickness, indicating that the two materials have comparable specific surface areas [22]. Moreover, Bustarret *et al.* [31,32] have shown that the nanostructure size of porous *a*-Si:H is about 3–5 nm thus similar to that of porous *c*-Si. Therefore we assume in the following that for a given sample (fixed doping level) the porosity and the size of the nanostructures are correlated, *i.e.*, the size of the nanostructures decreases with increasing porosity, as it has been observed by several groups for porous *c*-Si [33,34].

4 Results and discussion

4.1 In situ photoluminescence

In situ photoluminescence of porous silicon in HF is a crucial experiment for assessing size effects on the photoluminescence. The basic idea is to reduce the size of the silicon nanostructures *while* monitoring the PL signal. In crystalline silicon, as shown in a recent paper [10], the progressive shift of the PL during the reduction of the size gives a clear indication that the processes involved in recombination of a photocreated electron-hole pair are bulk recombination processes (quantum confinement effects). Note that if the luminescence were due to surface species [9] in our material, a progressive shift in *c*PS would not occur.

In *a*-Si:H, the situation is different. Because of the disordered nature of the material, the wave function of the carriers is localized [13]. Photocreated electron-hole pairs thermalize in the bandtails and get localized on a characteristic length of about 6–7 Å. Since the diameter of the silicon nanostructures is about 30 to 50 Å [32, 33] depending on the preparation conditions, no blueshift is expected when carrying out the same experiment with porous *a*-Si:H.

4.1.1 Crystalline silicon: the extended wavefunction

In situ PL of porous silicon in HF was qualitatively first mentioned by Canham [35] and has been studied by various groups [36–44]. In a recent paper [10], a detailed and comprehensive study of the *in situ* PL of crystalline silicon in HF has been carried out depending on the electrolyte

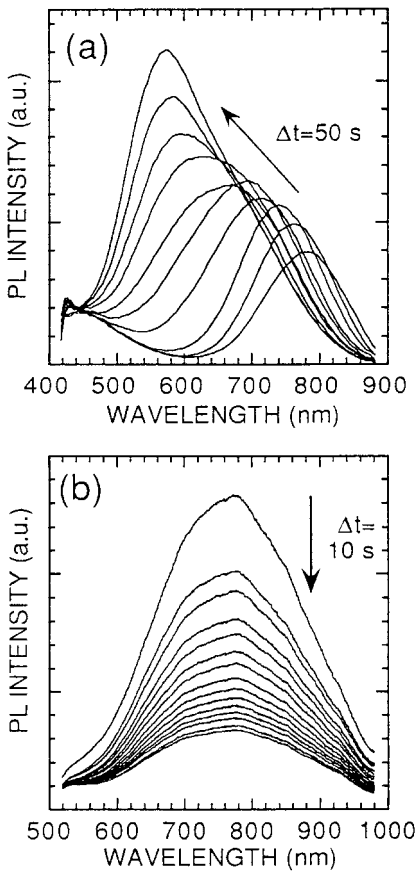

Fig. 5. Evolution of the *in situ* PL of *c*PS (a) and *a*PS (b) in ethanoic HF solution. Excitation 351 nm, 1.5 mW/cm^2 (a) and 20 mW/cm^2 (b). The direction of change and interval between two successive spectra are indicated in the figure. Note that the large blue shift is only present for *c*PS (neglecting the "statistical" blue shift).

composition, the excitation wavelength and intensity, investigating evolution rates and carrier lifetimes. Here, only the important results are reviewed in order to compare them with the measurements in porous amorphous silicon. A typical set of measurements was performed as follows: the cell was filled with alcoholic HF (HF:H_2O:EtOH (2:3:5)). Anodization was carried out with a current density of 20 mA/cm^2 for 5 minutes. This is thought to give a porous layer of ~ 5 μm thickness and a porosity of $\sim 65\%$ [10]. Then, either the same electrolyte was left in the cell, or, in order to minimize chemical etching effects of the porous structures, a different one was substituted without exposing the sample to air. Aging of the sample was studied under illumination of a krypton-ion laser beam while monitoring the PL. In order to suppress optical interferences in the porous layer, the initial silicon surface was poorly polished.

Figure 5a shows a typical evolution of porous silicon in HF. The initial luminescence of porous crystalline silicon in HF after anodization is centered around 800 nm and is generally lower by two to three orders of magnitude than that of a dry sample. After porous silicon formation, the laser excitation ($\lambda = 351$ nm) is switched on (here without exchange of the electrolyte) and successive spectra, equally time spaced ($\Delta t = 50$ s), are recorded. The spectra shift progressively to higher energies and reach a final state after a time $\tau \approx 500$ s with a peak wavelength around 560 nm. For very long illumination times the PL intensity starts to decrease.

The evolution from the red luminescence to the green luminescence is progressive. This simple observation stands as a strong argument in favor of a common origin for these luminescences. Since oxide species are known not to be stable in HF, the most straightforward interpretation for the evolution is that the photoluminescence of porous crystalline silicon is due to *quantum confinement effects*, and its blue shift under illumination in HF is related to photoelectrochemical etching (Appendix).

4.1.2 Remarks on the evolution of the PL intensities

The near-IR PL intensity of porous silicon is quenched by about 2 to 3 orders of magnitude in HF. Even if the exact reasons of this quenching are still a matter of debate [10,42], a plausible explanation is given by the screening effect on the photogenerated electron-hole pair, due to the high dielectric constant of the electrolyte [10].

During evolution, the ratio in PL intensity between the red and green peak intensities in Figure 5a is about a factor of 3 but it can be much larger in electrolytes with higher HF concentration. We have shown that the PL intensity increase is correlated with the PL blueshift [10]: when the size of the porous silicon structure is reduced, the probability to diffuse to a Shockley-Read-Hall center decreases, resulting in a lowering of the non-radiative recombination rate. Factors influencing the radiative efficiency (quantum efficiency, quenching by the liquid [10], ...) might also contribute to this effect.

4.1.3 Amorphous silicon: the localized wavefunction

The same experiment has been performed on *a*PS. We have anodized a 2 μm thick, *p*-doped (1.5% boron in gas phase) *a*-Si:H layer on stainless steel substrate (5 cm $\times$ 5 cm), in the cell described in the experimental section under the following conditions: current density of 10 mA/cm^2 and electrolyte concentration of 25% ethanoic HF. The resulting *a*PS layer has a thickness of about 0.4 μm and a porosity of about 75%. Then, for the same experimental conditions as for *c*PS (excitation: 351 nm, electrolyte: 25% ethanoic HF), the evolution of the PL as a function of the illumination time is monitored (Fig. 5b). After the laser is switched on, the initial luminescence of porous *a*-Si:H in HF is centered around 760 nm and is hardly quenched by the presence of the electrolyte, contrarily to what has been observed in *c*PS [10]. Then, a decrease of the luminescence intensity is observable, simply attributable to a loss of material, *without* any sizable blue shift (neglecting the "statistical" blue shift, see Sect. 4.3).

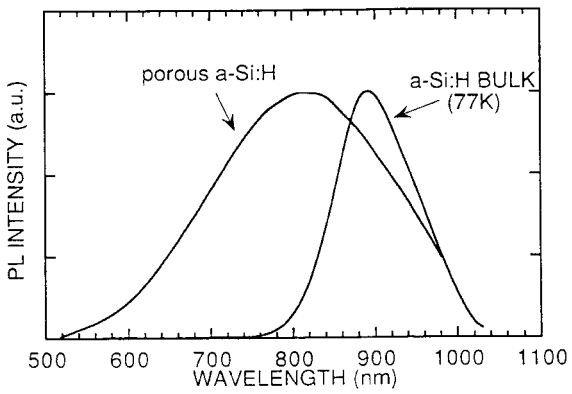

Fig. 6. Room-temperature photoluminescence spectrum of porous silicon obtained from *a*-Si:H under the following electrochemical conditions: 25% ethanoic HF, 10 mA/cm^2 current density. The PL spectrum of undoped bulk *a*-Si:H at T=77 K is added. Excitation 476 nm, 10 mW/cm^2. The PL intensities are scaled to the same peak intensity.

This experiment is *crucial* in the sense that it demonstrates the different quantum behavior of the photoluminescence of *a*PS and *c*PS: in *a*-Si:H, after excitation most carriers get trapped and are localized on a scale much smaller than the size of the porous structures. Hence, no blueshift occurs upon reducing the nanostructure size. In *c*-Si, where the wavefunction is extended, reducing the size of the structure results in a blue shift, showing clear evidence of quantum confinement effects.

4.2 High PL intensity and spatial confinement

A typical room-temperature PL spectrum of porous amorphous silicon (*a*PS) is shown in Figure 6. The PL was recorded under vacuum in order to avoid degradation effects. In the same way as for *c*PS, the samples of the highest porosity give the best room-temperature luminescence. The integrated intensity, after scaling to the layer thickness, is comparable to that of *c*PS, though generally somewhat lower (about one order of magnitude smaller) and the PL is homogeneous (down to 1 μm) under optical microscope. We now discuss the high PL intensity of *a*PS at room temperature in the spatial confinement model, as first proposed by Tiedje *et al.* [45] for thin layers and recently extended by Estes and Moddel [46] to small wires and dots.

At low temperature ($T \approx 50$ K), intrinsic bulk amorphous silicon is a highly luminescent material with a quantum efficiency of the order of 10% [47]. However, in highly boron doped *a*-Si:H, the material used for the fabrication of thick porous silicon layers, the low-temperature PL is strongly quenched due to the large amount of doping-related defects. For a defect density N_D of about 10^{18} cm^{-3}, it has been shown experimentally that the PL is quenched by about 4 orders of magnitude [26].

In the commonly used model of recombination in *a*-Si:H, first proposed by Street [26], defects provide the dominant recombination centers when their density is above 10^{17} cm^{-3} or when the temperature is higher than 100 K. At low temperature, photogenerated carriers thermalize in the bandtails and get trapped in localized states. Then, the electron-hole pairs can recombine either radiatively (see Sect. 4.6) or non-radiatively upon capture by a defect. Considering the distance from a defect at which the non-radiative and radiative recombination rates are equal, a nonradiative capture radius R_c around the defects can be defined. Alternately, R_c may be viewed as the characteristic distance explored by a photocreated electron-hole pair before its radiative recombination. The quantum efficiency is then determined by solving the nearest neighbor distribution function for randomly dispersed defects [26]. Then the quantum efficiency η_0 reads:

$$\eta_0 = \exp\left(-\frac{4}{3}\pi R_c^3 N_D\right) \tag{1}$$

where the non-radiative capture radius R_c is:

$$R_c = \frac{R_0}{2}\ln(\omega_0 \tau_R). \tag{2}$$

Here, N_D is the defect density, R_0 is the localization radius, ω_0 is the attempt-to-escape frequency ($\sim 10^{12}$ Hz) and τ_R is the radiative lifetime. This relationship has been experimentally verified by Tsang and Street [48] and recently by Schubert *et al.* [49]. They have fitted the data with a R_c of 100 to 120 Å, *i.e.*, a localization radius R_0 of about 10 Å, in good agreement with [13]. As depicted in Figure 7a, one can illustrate this model of non-radiative capture volumes of radius R_c by "dark spheres" surrounding defects. At low temperature, these dark regions are non-luminescent whereas the remaining space is highly luminescent with a quantum efficiency of about one ("light-gray space"). The quantum efficiency is then the ratio of the light-gray volume to the whole volume. For device-grade *a*-Si:H, the volume occupied by dark spheres is negligible, so that one observes very high quantum efficiencies ($\sim$ 10%) at low temperature. However, doping introduces defects and the total volume occupied by dark spheres increases. This accounts for the dramatic decrease of the quantum efficiency in strongly boron-doped *a*-Si:H.

In porous amorphous silicon the size of the structures is estimated to be in the range 30 to 50 Å [31,32]. In this nanostructured material, the probability for a photocarrier of encountering a non-radiative center is no more given by the dark-sphere volume but by the volume V_c of the intersection of the dark spheres with the nanostructure. When the characteristic size of the nanostructure is smaller than R_c, one has $V_c < 4\pi R_c^3/3$, hence the non-radiative recombination probability is decreased and the quantum efficiency is increased as compared to the bulk-case intensity (spatial confinement effect). In the limit that the size of the structures is much smaller than the capture radius ($d \ll R_c$), the result for 2D structures (planar layers), 1D structures (cylindrical wires) and 0D structures

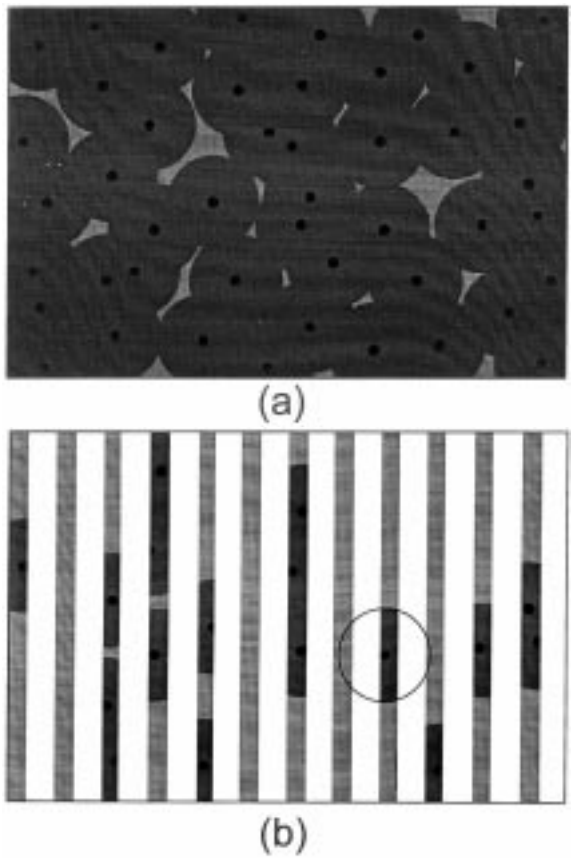

Fig. 7. Spatial confinement in amorphous silicon at low temperature. (a) illustrates the case of highly doped bulk *a*-Si:H. Dark spheres, representing non-radiative capture regions, cover almost the whole space. The quantum efficiency (ratio of light-gray space to the whole space) for, *e.g.*, a defect density $N_D = 10^{18}$ cm^{-3}eV^{-1}, is $\eta \simeq 10^{-3}$ (after Eq. (1)). In (b) the same bulk film has been etched into small wires (porosity $P = 60\%$). Since the structures are smaller than the non-radiative capture radius, the quantum efficiency increases: for the same defect density of $N_D = 10^{18}$ cm^{-3}eV^{-1}, (here for wires with a radius of 30 Å) $\eta = 50\%$ (Eq. (4)), *i.e.*, of about 3 orders of magnitude larger than in the bulk case. The circle in (b) has the size of dark spots of (a); it underlines the fact that the increased luminescence in (b) mainly arises from the much smaller volume surrounding centers in which recombination is non-radiative, the remainder of the initial volume being either non-existent or isolated from the centers by the voids.

(spherical particles) is:

$$\eta_{0,2D} = \exp\left(-\pi d R_c^2 N_D\right) \quad (d = \text{layer thickness}), \quad (3)$$

$$\eta_{0,1D} = \exp\left(-2\pi d^2 R_c N_D\right) \quad (d = \text{wire radius}), \quad (4)$$

$$\eta_{0,0D} = \exp\left(-\frac{4}{3}\pi d^3 N_D\right) \quad (d = \text{sphere radius}). \quad (5)$$

For device-grade material, this effect will not be very important, but for highly doped material, it leads to a dramatic increase of the quantum efficiency (Fig. 7b). For example, for a defect density $N_D = 10^{18}$ cm^{-3}, the PL efficiency is of the order of 10^{-3} for the bulk, whereas

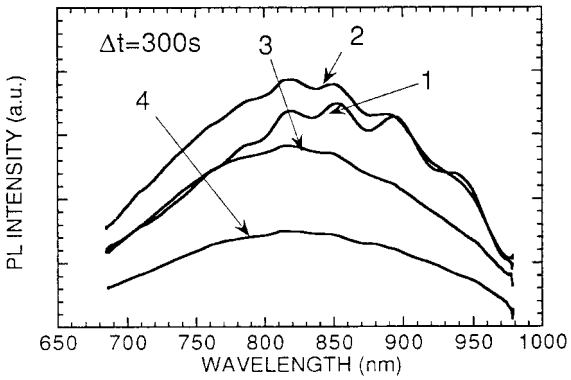

Fig. 8. Evolution of the *in situ* PL of low porosity *a*PS in 50% aqueous HF solution. Excitation 476 nm, 10 mW/cm^2. The successive spectra have been recorded in the order indicated in the figure. First an increase of intensity and a small "statistical" blue shift are observable and then the PL intensity decreases without any measurable blue shift.

for small wires ($d = 30$ Å), the PL efficiency increases to about 50%.

This picture of topological confinement would be invalidated if surface recombination in these small structures (wires or dots), with a large surface to volume ratio, would become dominant. In fact, silicon immersed in HF is perfectly passivated by hydrogen, as shown by Yablonovitch *et al.* [50], and exhibits extremely low surface-recombination velocities of about 1 cm/s which correspond to a center density of the order of 10^7 cm^{-2}. This nearly perfect electronic passivation survives as long as the hydrogen coating of the surface is stable. On *a*-Si:H, it is known that the surface hydrogen is much more stable than on *c*-Si [26]. The combination of the spatial confinement effect and a nearly perfect surface passivation is the key to understand the high PL intensity of porous amorphous silicon.

In the framework of the spatial confinement model, one expects that during *in situ* PL measurements, the PL intensity first increases by reducing the size (boron-doped bulk *a*-Si:H has a very low quantum efficiency), and then diminishes due to the etching of the structures and the corresponding loss of material. Indeed, this has been observed (see Fig. 8) when starting with a material of low porosity. We have anodized a 2 μm thick, *p*-doped (1.5% boron in gas phase) *a*-Si:H layer deposited on stainless steel under the following conditions: a current density of 10 mA/cm^2 and an electrolyte of 50% aqueous HF. The resulting porous layer has an initial porosity of about 45% and a thickness of about 0.1 μm. The photoelectrochemical etching is carried out in 50% aqueous HF and with the 476 nm line of the krypton-ion laser in order to have a slow evolution. Figure 8 shows a typical evolution, which is much slower than in 25% ethanoic HF. One observes a small increase of the PL intensity during the first minutes and then the same drop of the PL intensity as in Figure 5b. At the same time the interferences disappear from the spectrum, a further indication of the porous layer dissolution. As it will be discussed in the next section,

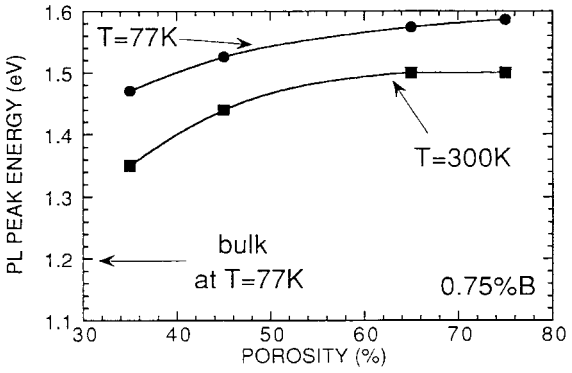

Fig. 9. Peak energy of the *a*PS PL spectra as a function of porosity at $T = 77$ K and 300 K.

the small blue shift observed in the spectra of Figure 8 is an expected feature, not related to quantum confinement effects.

In conclusion, *in situ* PL of porous *a*-Si:H can be fully explained by the spatial confinement model. The absence of a significant blue shift demonstrates that no quantum confinement effects are observable on the lowest localized states in *a*-Si:H.

4.3 The small "statistical shift" of the PL peak energy

The PL peak energy in device-grade bulk *a*-Si:H is known to be about 1.3 eV at low temperature and is estimated to be about 1.2 eV for boron-doped samples due to enlarged bandtails. In porous *a*-Si:H, the luminescence peak energy is observed at higher energies, at about 1.5 eV (Fig. 6). This shift is much smaller than the huge blue shift observed in *c*PS. Clearly, they are of different nature. We have analyzed the peak energy as a function of the porosity, *i.e.*, as experimentally shown for *c*PS [33,34], as a function of the size of the structures (see Sect. 3). For a fixed doping level (here about 0.75%), upon increasing the porosity, the PL peak energy shifts from 1.3 to 1.5 eV at room temperature and from 1.45 to 1.6 eV at low temperature (Fig. 9). A similar transition from about 1.4 to 1.5 eV has been observed upon photoelectrochemically etching low porosity samples in HF (Fig. 8).

In the PL model of Dunstan and Boulitrop [51], photocreated carriers thermalize in the bandtails and radiative recombination occurs in the critical volume V_c, from the deepest energy state of the conduction band to that of the valence band. Calculating the probability that an energy state is deepest within a sphere V_c, the density of deepest states $N_{deepest}(E)$ within volume V_c reads (here for the valence band, *i.e.*, "deepest states" means highest energy):

$$N_{deepest}(E) = N_0 \exp(-E/E_u^\nu) \times \exp(-V_c N_0 E_U^\nu \exp(-E/E_U^\nu)) \quad (6)$$

where E is counted from the valence band mobility edge, N_0 is the DOS at the mobility edge of the valence band and E_U^ν is the characteristic valence-bandtail energy. Since the PL spectrum is the convolution of the density of deepest energy states of the valence and the conduction band, the PL peak energy can be accounted for [51]:

$$E_{peak} = E_M - E_U^\nu \ln(V_c N_0 E_U^\nu) - E_U^c \ln(V_c N_0 E_U^c) \quad (7)$$

where E_M is the mobility gap. (The last two terms in Eq. (7) are the maxima of the densities for the valence and the conduction band, respectively). Tiedje *et al.* [45] and more recently Estes and Moddel [46] have expanded this model to 0D, 1D and 2D structures but the tendency is already observable from equation (7): when the volume V_c explored by the electron-hole pair decreases, the peak energy increases logarithmically towards the mobility edge. This purely statistical shift can be put in a more intuitive picture: when the electron-hole pair is confined in a small volume, the total number of available states in the bandtail becomes small, hence the lowest energy accessible to the pair before recombination is not as low as in the bulk material. For example, for $E_M = 1.7$ eV, $E_U^\nu \approx E_U^{optical} = 50$ meV and $N_0 = 10^{21}$ cm^{-3} eV^{-1}, one obtains a peak energy shift of about 0.2 eV from bulk *a*-Si:H to *a*-Si:H wires with a radius of $d = 1.5$ nm. This shift increases for higher Urbach energies and reaches about 0.35 eV for $E_U^\nu \approx E_U^{optical} = 100$ meV.

In Figure 9, for high porosities, *i.e.*, small sizes of the microstructures (see Sect. 3.), the dependence of peak energy on porosity becomes less pronounced at about 1.5 (resp. 1.6 eV) at room-temperature (resp. liquid nitrogen temperature), which is in good agreement with the logarithmic behavior (Eq. (7)). (Note that the *a*-Si:H gap changes by about 0.1 eV from 77 to 300 K [26]). This effect also accounts for the small PL peak shift observed during *in situ* PL (Fig. 8).

In summary, this small blue shift does not stem from quantum confinement effects, but is straightforwardly understood, as discussed above, from the availability of deep states in a restricted volume. Some recent numerical studies [52,53] have shown that quantum confinement effects in small *a*-Si:H dots or layers are theoretically possible. In order to understand the transition between pure spatial confinement and quantum confinement, we have undertaken a numerical simulation of a simple model featuring the effects of finite size and disorder on the states associated with a periodic potential. For the sake of simplicity, we have considered a one-dimensional Kronig-Penney (KP) model. Upon adding a random potential fluctuation with a standard deviation of 10% to the KP potential array, a bandtail appears in the density of states. This bandtail exhibits a nearly exponential decaying shape. This model is not adequate to describe the DOS in *a*-Si:H, but it shows qualitatively what happens to exponential bandtails and the ground state when the size of a structure is reduced. The statistical mean value of the ground-state energy for a large *a*-Si:H array (>100 sites) has an almost logarithmic dependence on the array size (Fig. 10). This is in good agreement with the model of Dunstan and Boulitrop (Eq. (7)). In the very simple KP model, the transition between the quantum confinement model ($1/d^2$-dependence)

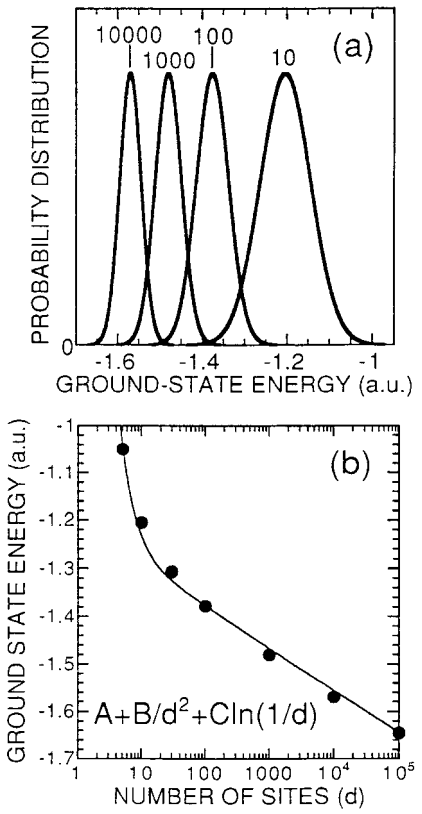

Fig. 10. (a) Calculated distribution of the ground state energy for different randomly created potential arrays. The number of sites in the array is indicated on the curves. (b) Averaged energy of the ground state for an array as a function of the array size. (10% RMS perturbation, average over 1000 ground state energies for different random distributions.) The line is a fit combining the quantum confinement model ($1/d^2$) and the statistical shift ($\ln(l/d)$).

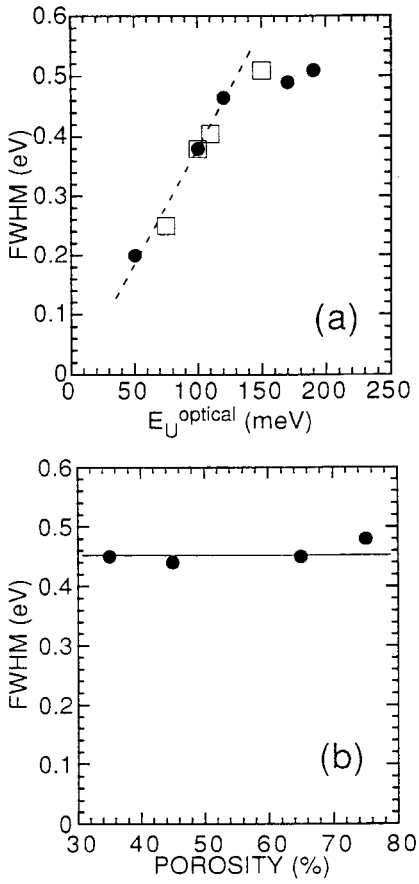

Fig. 11. (a) Full width at half maximum (FWHM) of porous *a*-Si:H PL spectra for different doping levels(0,0.1,0.2,0.75,1.5% boron in gas phase) and constant porosity (75%) as a function of the optically determined Urbach energy of the same layers before anodization (filled circles). The FWHM of $a\mathrm{Si}_{1-x}C_x$:H PL spectra of reference [54] are shown (squares). Based on equation (8), a linear fit for all data points below $E_U^{optical}$ <150 meV is inserted. (b) The FWHM of *a*PS is plotted as a function of porosity (35%, 45%, 65%, 75%) for a constant doping level (0.75% boron in gas phase).

and the spatial confinement model $\ln(1/d)$-dependence) is observed for very small arrays ($\leq$ 10 sites). Even though the calculation is not quantitative, first-principle considerations (localization length of about 6–7 Å whereas the *a*PS structure sizes are between 30–50 Å [32]) and the recent quantitative empirical tight-binding calculation of Allan *et al.* [53] (significant HOMO-LUMO gap increase only for slabs smaller than 1 nm) support that no quantum confinement effects are possible for the structure sizes present in porous amorphous silicon.

4.4 Width of the PL spectrum

In the same model of Dunstan and Boulitrop [51], the full width at half maximum (FWHM) of the PL can be estimated from the width of the density of deepest states. The distribution width ΔE can be obtained numerically from equation (6) (here for the valence band):

$$\Delta E^{\nu} \cong 2.5 E_U^{\nu}. \tag{8}$$

Experimentally available are the full width at half maximum of the spectra (FWHM) and the optically determined Urbach energy $E_U^{optical}$. These are not exactly the same values as ΔE^{ν} and E_U^{ν}: the PL spectrum (resp. the optical absorption) involves a convolution of the distribution $N_{deepest}(E)$ (Eq. (6)) (resp. the DOS weighted with dipole-matrix element) of the valence band with that of the conduction band. Since these two convolutions operate on mathematically different functions, the resulting scaling factor may be different for ΔE and E_U, hence, the theoretical slope of 2.5 in equation (8) gives only an order of magnitude estimate. Experimentally, a value of 3.85 for the prefactor in equation (8) has been determined for a-Si_{1-x}:C_x:H alloys [54].

In Figure 11a, the width of the spectrum (FWHM) of several *a*PS samples obtained from differently doped *a*-Si:H layers, but with a fixed porosity of about 70%, is plotted against the optically determined Urbach energy of the same *a*-Si:H layers *before anodization.* (The porous *a*-Si:H layers are too thin for a direct determination

of E_U.) The FWHM of the PL increases with disorder and we find exactly the same dependence of the FWHM on the Urbach energy as for the carbon-silicon alloys taken from [54]. This is a strong argument that the density of states in porous a-Si:H is the same as in bulk a-Si:H before anodization.

This is supported by the fact that varying the porosity for a fixed doping level does not change the FWHM of the PL (Fig. 11b). Relating nanostructure size and porosity is not straightforward and may depend upon sample preparation (*e.g.*, doping level). However, for a given sample, increasing the porosity leads to decreasing nanostructure size (see Sect. 3). Therefore, interpretations of size effects on the density of states in a-Si:H nanostructures [14,19, 55] are ruled out by the present experiment [56].

4.5 Temperature dependence of the photoluminescence

In an ideal nanosphere, perfectly insulated from the rest of the material, and containing no defects, the PL quantum efficiency is unity and independent of temperature. If such a nanoparticle is connected to the rest of the porous material, the situation is different: as soon as diffusion in the mobility band (a thermally activated process) becomes possible, a nonradiative capture by a defect will unavoidably take place and the PL will be strongly quenched, as in bulk a-Si:H. The existence of a strong thermal quenching of the PL then stands as a clear-cut proof of the connectivity of the porous structure.

In the dark-spot model (Sect. 4.2), an electron-hole pair in a bright region can diffuse and eventually reach a dark spot when the temperature is increased. This results in a decrease of the PL ("thermal quenching"). In a simple model, one can suppose that each carrier which is reemitted from a trap recombines non-radiatively. Then, thermal quenching occurs for all carriers for which the thermal reemission rate is higher than the radiative recombination rate $1/\tau_R$. Equating these rates, one obtains a critical energy, called demarcation energy $E_D(T, \tau_R)$:

$$E_D(T, \tau_R) = E_M - kT \ln(\omega_0 \tau_R) \tag{9}$$

where ω_0 is a characteristic attempt-to-escape frequency ($\sim 10^{12}$ s^{-1}). By calculating the proportion of carriers which are trapped deeper than E_D, one obtains for the temperature-dependent quantum efficiency [26]:

$$\eta(T) \propto \exp\left(-kT \frac{\ln(\omega_0 \tau_R)}{E_U}\right) = \exp\left(-\frac{T}{T_0}\right) \tag{10}$$

with

$$kT_0 = \frac{E_U}{\ln(\omega_0 \tau_R)} \approx \frac{1}{20} E_U \tag{11}$$

for a radiative recombination time τ_R of about 1 ms. In this simple model, the high-temperature PL intensity obeys an exponential law described by a characteristic temperature T_0 proportional to the Urbach energy E_U.

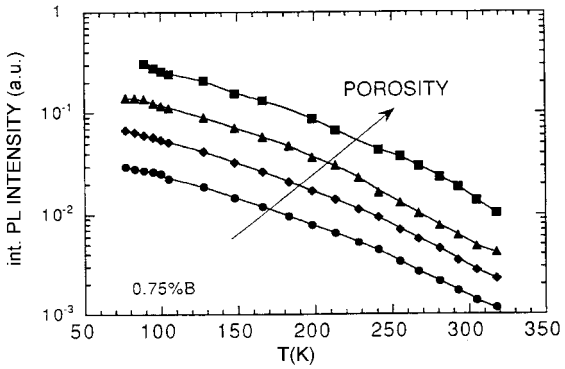

Fig. 12. Temperature dependence of the integrated PL intensity for aPS of different porosities. Here, the porosity is successively changed from 35%, 45%, 65%, to 75%) by varying the HF concentration with a fixed doping level (0.75% B).

In a more detailed model, including the diffusion capability of the electron-hole pair, we have shown that the temperature dependence of the quantum efficiency in the high-temperature limit is similar to equation (10) [22,25]. However, in order to extend the fit of the PL intensity towards low T (down to about 50 K), the simple law in equation (10) has to be complemented. Experimentally, it was found that [57]

$$\eta(T) = \frac{A}{1 + B \exp(T/T_0)} \tag{12}$$

fits the PL data over a wide temperature range.

In the standard model of thermal quenching (Eq. (10)), spatial confinement is not expected to affect the escape probability of an electron or hole trapped in the bandtails. On the opposite, quantum effects on the extended states in amorphous silicon might increase the Urbach energy due to the spreading of the bandtail and therefore lower the escape probability (this has been taken as evidence for quantum confinement effects in a-Si:H multilayers [17]). In a simple model, diffusion and subsequent capture of the electron-hole pair by a Shockley-Read-Hall center may be considered independent of confinement. Then, without quantum effects, the PL yield $\eta(T)$ in a small a-Si:H particle is just proportional to that of bulk a-Si:H, where as with quantum effects, T_0 should increase and the PL should depend less on the temperature than that of bulk a-Si:H.

Photoluminescence (PL) of amorphous porous silicon (aPS) has been recorded as a function of temperature (from 77 K to 400 K) for layers formed under various conditions of a-Si:H doping (from 0.1% to 3% boron in gas phase) and HF concentration (from 5 to 50%). It has been checked that the PL intensity is a linear function of the excitation intensity for intensities up to at least 150 mW/cm^2 for blue excitation ($\lambda = 476$ nm) and up to 20 mW/cm^2 for UV excitation ($\lambda = 351$ nm), excluding Auger effects.

Figure 12 shows the temperature dependence for different porosities obtained by porous etching of bulk material at different HF concentrations for a *fixed doping level*.

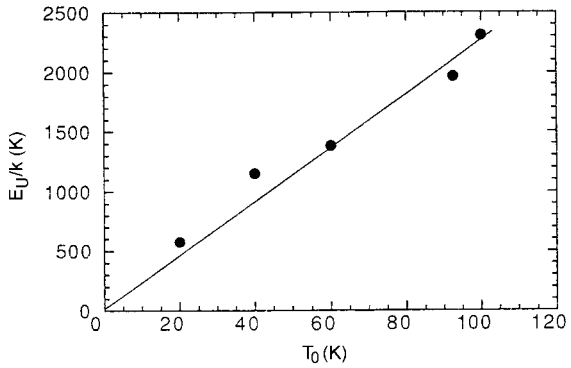

Fig. 13. Urbach energy determined by photospectrometry as a function of the characteristic temperature T_0 determined by the temperature-dependence of the PL. All samples have a porosity of 70%, but are made from bulk materials of different doping levels (undoped, 0.1, 0.2, 0.75 and 1.5%). Higher doping levels correspond to larger Urbach energies. According to theory, T_0 is expected to be proportional to E_U.

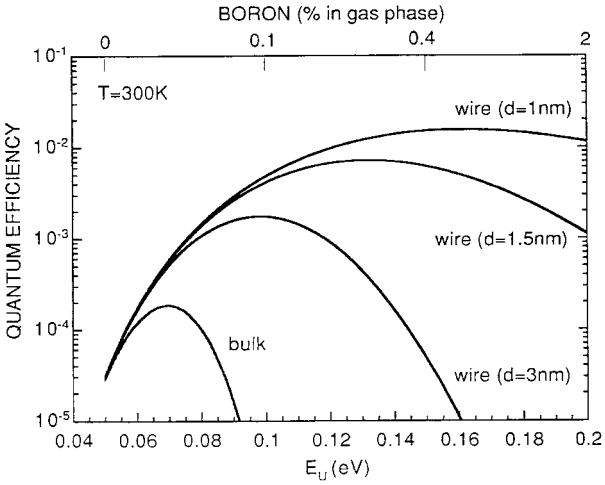

Fig. 14. Calculated PL quantum efficiency at T=300 K after equations (13, 14) for bulk a-Si:H wires (radius d = 1, 1.5 and 3 nm) as a function of the Urbach energy.

A strong thermal quenching of the PL signal is observed for all porosities. By the way this confirms that aPS consists of interconnected dots or a skeleton of wires as in crystalline silicon rather than isolated nanoparticles. In the high-temperature range, one clearly observes that the slope, *i.e.*, the characteristic temperature T_0 (Eq. (11)), is independent of the porosity. Varying the size of the structures has therefore no influence on T_0 , *i.e.*, on the Urbach energy.

However, the value of T_0 in our bright-luminescent sample is larger than for undoped bulk solids (100 K instead of 20 K). These results are in typical agreement with those of Bustarret *et al.* [3,31] assuming a value of $T_0 \approx 150$ K for Bustarret's samples, that are more heavily doped than ours [1]. Therefore, we have made a systematic study of T_0 depending on the doping level of aPS (for a nearly fixed porosity except for the bulk case). Plotting the Urbach energy E_U (determined by optical absorption measurements) *versus* T_0 (determined from the temperature dependent PL data using Eq. (12)) for doping levels between 0 and 1.5% boron in gas phase, yields a straight line (Fig. 13) with a slope of about 23. This is in excellent agreement with the estimated value of about 20 for a radiative recombination time of about 1 ms. Even for a shorter radiative lifetime, the constant will hardly change due to its logarithmic dependency, *e.g.* for $\tau_R = 10^{-6}$ s, one obtains a proportionality constant of 14, still in fair agreement with the data in view of the oversimplification of the models, (*e.g.*, our implicit assumption that the electron-hole pair moves as a single entity).

In summary, the weaker temperature dependence in p-type a-Si:H in comparison with intrinsic a-Si:H can be fully explained by the fact that boron doping introduces a higher disorder in the material. The more the Urbach energy is enlarged, the more the luminescence is independent of temperature, a similar effect as in a-Si_{1-x}:C_x:H [54]. This explains why in a preliminary study [22], we had observed an increase in T_0 when changing the porosity by varying the doping level.

We now analyze the PL quantum efficiency at room-temperature in detail. Since the low-temperature quantum efficiency (Eqs. (1–5)) and the high-temperature quenching effect (Eqs. (10, 11)) are both decreasing with increasing doping, there is a doping level for which the quantum efficiency at room temperature is maximum. In the high-temperature limit, the quantum efficiency can be approximated by

$$\eta = \exp(-V_c N_D) \exp(-T/T_0). \tag{13}$$

Now, we need a relationship between the characteristic temperature T_0, *i.e.*, the Urbach energy E_U (Eq. (11)) and the defect density N_D. This relationship is given by the weak-bond-dangling-bond conversion model, proposed by Stutzmann [58]:

$$N_D = N_0 E_U \exp(-E_{db}/E_U) \tag{14}$$

where a value E_{db} of about 0.4 eV has been obtained experimentally.

Thus from equations (13, 14), we can calculate the room-temperature quantum efficiency depending on the Urbach energy, *i.e.*, on the doping level. In Figure 14, one observes that for bulk a-Si:H the maximal quantum efficiency is obtained for Urbach energies corresponding to low doping levels and the absolute QE is rather low (10^{-4}). For small wires ($V_c = 2\pi d^2 R_c$), the situation is different. Here the optimum doping level is shifted to larger Urbach energies, *i.e.*, higher boron concentration, and the absolute QE is increasing. Note that for small wires with a radius of about 10 Å, the QE at room-temperature can be as high as 1%. This simple model explains qualitatively why strongly light-emitting porous a-Si:H samples have been obtained only from highly boron-doped a-Si:H films [1,6,7].

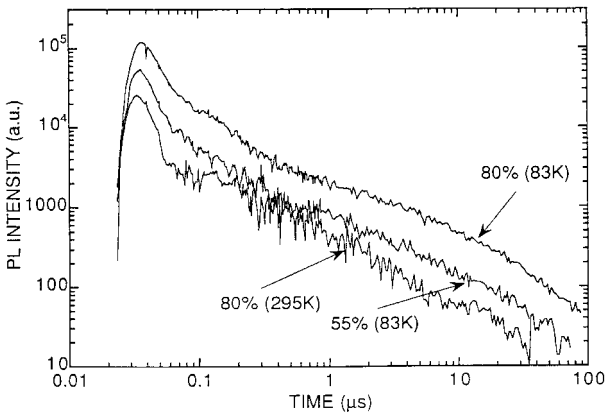

Fig. 15. Time-resolved photoluminescence measurements of porous a-Si:H for different porosities and temperatures (see values on the curves). The doping level is fixed at 1.5% boron in gas phase.

In summary, spatial confinement determines the low temperature quantum efficiency, whereas the degree of disorder in the structures (introduced by boron) determines the PL quenching at higher temperature. No quantum confinement effects on the Urbach energy can be detected.

4.6 Photoluminescence decay

Time-resolved photoluminescence measurements have been carried out for samples with a doping level of about 1.5%. Figure 15 shows the PL decays of aPS for two different porosities (55% and 80%) and two different temperatures (83 K and 295 K). The decays have essentially the same non-exponential shape and the same average lifetime [59] of about 1 μs, defined by

$$\tau = \frac{1}{I_{max}} \int_0^\infty I(t)dt. \tag{15}$$

Since the lifetime does not depend on temperature, it is concluded that the lifetime of 1 μs is the radiative lifetime. This observation stands in contrast to the temperature dependence of the average lifetime in crystalline porous silicon where a decrease of about one order of magnitude has been reported from about 100 μs at 77 K to about 10 μs at 300 K [59]. In *oxidized* aPS, the average lifetime is found to be 10–30 μs, and weakly temperature dependent [31].

In amorphous silicon, time-resolved data are generally interpreted according to the attempt of Tsang and Street [48]. In their model, a distribution $G(\tau)$ of exponential lifetime decays $\exp(-t/\tau)$ accounts for the decay profile. For the low temperature decays in Figure 15, the lifetime distributions of the aPS samples have a maximum at about 1 μs, independently of the porosity.

In device-grade a-Si:H, the lifetime distribution peaks at about 10^{-3} and 10^{-6} s [60]. The radiative lifetime of our aPS samples seems to coincide with the short radiative lifetime in bulk a-Si:H. Due to the small thickness of the aPS films, the signal-to-noise ratio of our measurements was not sufficient to analyze the millisecond region.

In summary, we have detected a radiative lifetime of about 1 μs in aPS. There is no significant change in the lifetime from 55% to 80% porosity, therefore no apparent change of the lifetime when the size of the structures is reduced (see Sect. 3), which is in apparent contradiction with the tunneling recombination model [26,46].

5 Comparison between the PL properties of porous amorphous silicon and ultrathin a-Si:H multilayers

Abeles and Tiedje [61] and Miyazaki *et al.* [14] have observed a small PL-peak-energy blue shift of about 0.1 eV (1.3 to 1.4 eV) when reducing the well width of their ultrathin a-Si:H multilayer structures. Whereas Miyazaki *et al.* [14] interpret this shift as a quantum confinement effect on the localized states (based on theoretical works by Tsu [62]), Tiedje *et al.* [45] explain this small shift by a statistical effect on the bandtail density of states, as described in Section 4.3. Recently, Lockwood *et al.* [15] observed a size dependence of the PL emission energy of a-Si/SiO_2 multilayers (1.7 eV to 2.3 eV), in fair agreement with QCE. However, these results have not been reproduced yet.

An increase of the Tauc gap and the Urbach energy E_U with decreasing layer thickness has been detected by optical absorption measurements on ultrathin a-Si:H/a-Si_{1-x}:N_x:H multilayers [14,17,18,55]. A similar increase of the characteristic temperature T_0 obtained from temperature dependent PL measurements has been observed when reducing the size of the a-Si:H layer [17]. These results have been interpreted as evidence that the extended states, and therefore indirectly the bandtail density of states, are affected by quantum confinement effects (see *e.g.*, Abeles and Tiedje [61], Miyazaki *et al.* [14]).

Recently, other interpretations of the optical measurements on a-Si:H multilayers have emerged [20,62–64]. A higher Urbach energy is also an indication for higher disorder. Interfaces at the multilayer structures might introduce additional disorder, resulting in an increase of the Urbach energy [21]. Moreover, a study of ultrathin single a-Si:H layers by Koehler and Fritzsche leads to the conclusion that no QCE effects can be observed [63]. They conclude that the thin structures have a *different morphology* [21], *i.e.*, a density lower than bulk a-Si:H, resulting in a higher disorder and therefore a higher Urbach energy. Other groups object by saying that the standard method of determining the Tauc gap in a-Si:H can introduce a large error if multilayers are used since normally used *effective medium* approaches can fail [64] or even the Tauc gap definition is not adequate and has to be replaced by the Cody gap definition [65]. Clearly, interface and morphology problems severely complicate the interpretation of the experimental data recorded on multilayers. Porous amorphous silicon has several advantages in comparison to multilayers: porous amorphous silicon consists of 0D or 1D structures in contrast with 2D confinement in multilayers

(higher confinement degree). It has the same atomic structure as bulk amorphous silicon since it is obtained from it by anodic etching. The *a*PS structures are freestanding (no barrier material) and, due to the high hydrogen surface passivation, they have almost no interface states.

In the analysis of recombination properties of *a*-Si:H nanostructures, one has to distinguish between the PL properties which affect the lowest localized states responsible for the PL peak energy, and those which concern the extended states and therefore indirectly the Urbach energy. It has been shown by *in situ* PL that the luminescences of *a*PS and *c*PS behave differently because of the medium range disorder of the amorphous material. There is clear evidence that the lowest localized states in *a*PS, responsible for the PL, are not affected by quantum effects. The small PL blue shift observed upon increasing porosity has been consistently explained by the statistical shift in perfect agreement with the results of Tiedje *et al.* on *a*-Si:H multilayers [45]. Contrarily to investigations on *a*-Si:H multilayers, the temperature dependent measurements and the analysis of the width of the spectrum of *a*PS exclude a spreading of the *a*-Si:H bandtail as a consequence of quantum confinement effects.

Therefore, our results favor the interpretation that interfaces or a lower material density cause the increase of the Urbach energy in *a*-Si:H multilayers.

6 Summary and conclusions

High PL intensity at low T in porous *a*-Si:H has been consistently explained in the model of spatial confinement: when the *a*-Si:H structures are made smaller than the mean capture radius of a defect, the probability for an electron-hole pair to recombine non-radiatively decreases strongly. At room temperature in boron-doped samples, the competition between spatial confinement and enlarged bandtails determines the optimum PL intensity. In comparison to the bulk where the optimum PL intensity occurs for nearly intrinsic material, the optimum in small wires is shifted to high doping levels (1%). This explains why room-temperature PL of porous *a*-Si:H has first been observed in strongly doped *a*-Si:H.

The comparison between the photoluminescence (PL) properties of amorphous and crystalline silicon provides clear-cut information on the nature of PL in both types of materials. For porous crystalline silicon, when the size of the nanostructures is decreased (by photoelectrochemical etching), a huge blue shift (from 1.5 to 2.3 eV) is observed until, eventually, the whole layer is etched out. The same experiment performed on porous amorphous silicon shows a decrease of the PL intensity with the loss of material, but without any significant blue shift. Because of disorder, the electron wavefunctions in amorphous silicon are localized within about 10 Å (Mott-Anderson localization). Thus, it is not expected that the PL peak energy changes when the size of the structures is reduced, which is indeed evidenced by the *in situ* measurements in HF. For crystalline porous silicon the large variation of the PL peak energy measured *in situ* during photoelectrochemical etching can be understood in terms of quantum confinement effects: photoelectrochemical etching reduces the sizes of the structures and increases the bandgap. This model of wave-function confinement is strongly supported, *ab absurdo*, by the fact that no shift is observed with the same experiment performed on the same material but now in a disordered state, where the wavefunction is already localized. The same results can be regarded as a very direct experimental proof of the Mott-Anderson localization in hydrogenated amorphous silicon, with a localization length of a few atomic distances.

When the porosity of porous amorphous silicon is varied from 35% to 75%, a small blue shift of the peak energy from about 1.3 to 1.5 eV is observed. This small blue shift is clearly distinct from the huge blue shift in porous crystalline silicon and can be entirely explained by a statistical effect on the availability of the bandtail states: when the size of the structures is reduced, the probability for an electron-hole pair to find a state as deep as in the bulk material decreases.

The temperature dependence of the PL of porous *a*-Si:H is identical to that of bulk amorphous silicon. These experiments demonstrate that the Urbach energy is preserved when the size of the porous *a*-Si:H nanostructures is reduced, excluding quantum effects on the bandtail density of states. These results are supported by the analysis of the width of the spectrum and stand in clear contrast with interpretations of quantum confinement effects in ultrathin *a*-Si:H multilayers.

R.B.W. would like to thank Prof. G.H. Bauer for stimulating discussions and support during the early part of this work. We are grateful to I. Mihalcescu for parts of the time-resolved measurements and D. Bellet for the X-ray measurements.

Appendix : Photoelectrochemical etching

When an electron-hole pair is photocreated in a small silicon particle, different recombination paths may occur.

For a *dried* porous silicon sample in air, photocarriers recombine either radiatively or non-radiatively. In the presence of an *electrolyte*, an alternate path for carrier annihilation is the consumption in an electrochemical reaction. Note that the charge neutrality requires that both carriers undergo an electrochemical reaction. Eventhough the net current is zero, this is an essentially electrochemical mechanism, and the term of photoelectrochemical etching is more appropriate than that of photoetching. In a simplified picture [10], photoelectrons reaching the surface will result in hydrogen evolution (decomposition of the electrolyte) according to the scheme

$$2e^- + 2\mathrm{H}^+ \rightarrow \mathrm{H}_2 \uparrow .$$

On the other hand, holes reaching the surface cause silicon dissolution *via*

$$2h^+ + \mathrm{Si} + 6\mathrm{HF} \rightarrow \mathrm{SiF}_6^{2-} + 4\mathrm{H}^+ + \mathrm{H}_2 \uparrow .$$

According to the commonly accepted ideas about silicon dissolution in HF, it is also possible that a single hole reaching the surface might result in dissolution of one silicon atom, since a hole is needed only for the first step, and the next step may take place through electron injection in the conduction band [66,67]:

$$h^+ + \mathrm{Si} + 6\mathrm{HF} \rightarrow \mathrm{SiF}_6^{2-} + e^- + 4\mathrm{H}^+ + \mathrm{H}_2 \uparrow .$$

In any case, silicon will be photoetched, at a rate corresponding to one silicon atom for every one or two photoholes reaching the surface.

References

1. E. Bustarret, M. Ligeon, L. Ortega, Solid State Commun. **83**, 461 (1992).
2. E. Bustarret, J.-C. Bruyère, F. Muller, M. Ligeon, Mat. Res. Soc. Symp. Proc. **283**, 39 (1993).
3. E. Bustarret, M. Ligeon, M. Rosenbauer, Phys. Stat. Sol. (b) **190**, 111 (1995).
4. K.H. Jung, S. Shih, D.L. Kwong, C.C. Cho, B.E. Gnade, Appl. Phys. Lett. **61**, 2467 (1992).
5. A.I. Yakimov, N.P. Stepine, A.V. Dvurechenskii, L.A. Scherbakova, Physica B **205**, 298 (1995).
6. R.B. Wehrspohn, J.-N. Chazalviel, F. Ozanam, I. Solomon, Phys. Rev. Lett. **77**, 1885 (1996).
7. M.J. Estes, L.R. Hirsch, S. Wichardt, G. Moddel, J. Appl. Phys. **82**, 1832 (1997).
8. R.B. Wehrspohn, J.-N. Chazalviel, F. Ozanam, I. Solomon, Thin Solid Films **297**, 5 (1997).
9. L.T. Canham, Phys. Stat. Sol. (b) **190**, 9 (1995) and references therein.
10. F. Ozanam, J.-N. Chazalviel, R.B. Wehrspohn, Thin Solid Films **297**, 53 (1997); J.-N. Chazalviel, F. Ozanam, in *Structural and Optical Properties of Porous Silicon Nanostructures*, edited by G. Amato, C. Delerue, H.J. von Bardeleben (Gordon & Breach, Amsterdam, The Netherlands, 1997), p. 53.
11. P.D.J. Calcott, K.J. Nash, L.T. Canham, M.J. Kane, D. Brumhead, J. Phys.-Cond. **5**, L91 (1993).
12. A. Bsiesy, F. Muller, M. Ligeon, F. Gaspard, R. Herino, R. Romestain, J.C. Vial, Phys. Rev. Lett. **71**, 637 (1993).
13. N.F. Mott, Philos. Mag. B **43**, 941 (1981); N.F. Mott, E.A. Davies, *Electronic processes in Non-crystalline Materials* (Clarendon, Oxford, 1979), p. 24.
14. S. Miyazaki, K. Yamada, M. Hirose, J. Non-Cryst. Sol. **137-138**, 1119 (1991).
15. D.J. Lockwood, Z.H. Lu, J.-M. Baribeau, Phys. Rev. Lett. **76**, 537 (1996).
16. M.E. Raikh, S.D. Baranovskii, B.I. Shklovskii, Phys. Rev. B **41**, 7701 (1990).
17. B. Abeles, T. Tiedje, Phys. Rev. Lett. **51**, 2003 (1983).
18. S. Miyazaki, M. Hirose, in *Amorphous and Microcrystalline Semiconductor Devices: Optoelectronic Devices*, edited by J. Kanicki (Artech, Boston, 1991), p. 180.
19. F. Yonezawa, F. Satoh, Philos. Mag. B **60**, 109 (1989).
20. R.W. Collins, C.-Y. Huang, Phys. Rev. B **34**, 2910 (1986).
21. R.W. Collins, B.Y. Yang, J. Vac. Sci. Technol. B **7**, 1155 (1989).
22. J.-N. Chazalviel, R.B. Wehrspohn, F. Ozanam, I. Solomon, Mat. Res. Soc. Symp. Proc. **452**, 403 (1997).
23. I. Solomon, R.B. Wehrspohn, J.-N. Chazalviel, F. Ozanam, J. Non-Cryst. Sol. **227-230**, 248 (1998).
24. F. Ozanam, R.B. Wehrspohn, J.-N. Chazalviel, I. Solomon, Phys. Stat. Sol. (a) **165** (1998).
25. R.B. Wehrspohn, Ph.D. thesis, École Polytechnique, Palaiseau, France, 1997.
26. R.A. Street, *Hydrogenated amorphous silicon* (Cambridge Solid State Science Series, Cambridge, UK, 1991) and references therein.
27. I. Solomon, M.P. Schmidt, H. Tran-Quoc, Phys. Rev. B **38**, 9895 (1988); I. Solomon, M.P. Schmidt, C. Sénémaud, M. Driss Khodja, *ibid.* **38**, 13263 (1988).
28. I. Solomon, R. Benferhat, H. Tran-Quoc, Phys Rev. B **30**, 3422 (1984).
29. R.L. Smith, S.D. Collins, J. Appl. Phys. **71**, R1 (1992).
30. W.W. Mullins, R.F. Sekerka, J. Appl. Phys. **35**, 444 (1964).
31. E. Bustarret, E. Sauvain, M. Ligeon, M. Rosenbauer, Thin Solid Films **276**, 134 (1996).
32. E. Bustarret, E. Sauvain, M. Ligeon, Philos. Mag. Lett. **75**, 35 (1997).
33. M. Binder, T. Edelmann, T.H. Metzger, G. Mauckner, G. Goerigk, J. Peisl, Thin Solid Films **276**, 65 (1996).
34. J. von Behren, T. van Buuren, M. Zacharias, E.H. Chimowitz, P.M. Fauchet, Solid State Commun. **105**, 317 (1998)
35. L.T. Canham (private communication, 1992).
36. V.M. Dubin, F. Ozanam, J.-N. Chazalviel, Phys. Rev. B **50**, 14867 (1994).
37. A. Kux, F. Müller, F. Koch, Mat. Res. Soc. Symp. Proc. **283**, 311 (1993).
38. R. Wielgosz, L.M. Peter (private communication).
39. T. Wadayama, S. Yamamoto, A. Hatta, Appl. Phys. Lett. **65**, 1653 (1994); *ibid.* **66**, 2913 (1995).
40. M. Davison, K.P. O'Donnell, U.M. Noor, D. Uttamchandani, L.E.A. Berlouis, Appl. Phys. Lett. **66**, 2912 (1995).
41. T. Ichinohe, S. Nozaki, H. Ono, H. Morisaki, Appl. Phys. Lett. **66**, 1644 (1993).
42. S. Létant, J.C. Vial, J. Appl. Phys. **80**, 7018 (1996).
43. H. Mizuno, H. Koyama, N. Koshida, Appl. Phys. Lett. **69**, 3779 (1996).
44. K.-H. Li, C. Tsai, J. Sarathy, J.C. Campbell, Appl. Phys. Lett. **62**, 3192 (1993).
45. T. Tiedje, B. Abeles, B.G. Brooks, Phys. Rev. Lett. **54**, 2545 (1985).
46. M.J. Estes, G. Moddel, Appl. Phys. Lett. **68**, 13 (1996); M.J. Estes, G. Moddel, Phys. Rev. B **54**, 14633 (1996).
47. W.B. Jackson, R.J. Nemanich, J. Non-Cryst. Sol. **59-60**, 353 (1983).
48. C. Tsang, R.A. Street, Phys. Rev. B **19**, 3027 (1979).
49. M. Schubert, R. Stachowitz, W. Fuhs, Phys. Rev. B **52**, 10906 (1995).
50. E. Yablonovitch, D.L. Allara, C.C. Chang, T. Gmitter, T.B. Bright, Phys. Rev. Lett. **57**, 249 (1986).
51. D.J. Dunstan, F. Boulitrop, Phys. Rev. B **30**, 5945 (1984).
52. G. Allan, C. Delerue, M. Lannoo, Phys. Rev. Lett. **78**, 3161 (1997).
53. G. Allan, C. Delerue, M. Lannoo, Appl. Phys. Lett. **71**, 1189 (1997).
54. L.R. Tessler, I. Solomon, Mat. Res. Soc. Symp. Proc. **336**, 613 (1994).
55. M. Yamaguchi, K. Morigaki, Phys. Rev. B **55**, 2368 (1997).

56. The analysis of the Kronig-Penney calculation supports the model of preserved Urbach energies. The width of the probability distribution of the ground state in the KP model as a function of the array size was calculated from Figure 10a. An almost constant FWHM for all sizes can be observed. Only for very small arrays (<10 potential wells), the FWHM increases strongly due to a change in the Urbach energy caused by quantum confinement effects. This onset coincides with the transition from a $\ln(1/d)$ to a $1/d^2$ dependence in the mean ground-state energy.
57. R.W. Collins, M.A. Paesler, W. Paul, Solid State Commun. **34**, 833 (1980).
58. M. Stutzmann, Philos. Mag. B **60**, 531 (1989).
59. J.C. Vial, in *Porous Silicon Science and Technology*, edited by J.C. Vial, J. Derrien (Les Éditions de Physique, Les Ulis, 1995), p. 137.
60. T. Muschik, R. Schwarz, J. Non-Cryst. Sol. **164-166**, 619 (1993).
61. B. Abeles, T. Tiedje, in *Semiconductors and Semimetals*, edited by J.I. Pankove (Academic, New York, 1984).
62. R. Tsu, J. Non-Cryst. Sol. **114**, 708 (1989).
63. S. A. Koehler, H. Fritzsche, Mat. Res. Soc. Symp. Proc. **420**, 741 (1996).
64. N. Bernhardt, G.H. Bauer, Phys. Rev. B **52**, 8829 (1995).
65. M. Beaudoin, M. Meunier, C.J. Arsenault, Phys. Rev. B **47**, 2197 (1993).
66. H. Gerischer, P. Allongue, V. Costa Kieling, Ber. Bunsenges. Phys. Chem. **97**, 753 (1993).
67. V. Lehmann, U. Gösele, Appl. Phys. Lett. **58**, 856 (1991).